JOURNAL OF GUIDANCE, CONTROL, AND DYNAMICS
Vol. 46, No. 12, December 2023

Adaptive Force-Control Augmentation for Small Celestial Body Sampling

Nima Mohseni* and Dennis S. Bernstein†
University of Michigan, Ann Arbor, Michigan 48109
and
Marco B. Quadrelli‡
Jet Propulsion Laboratory, California Institute of Technology, Pasadena, California 91109

https://doi.org/10.2514/1.G007575

An adaptive force-control augmentation for small celestial body sampling for a variety of surface properties is developed. The control algorithm consists of a nominal robust controller augmented with an adaptive controller combined with feedback linearization. When a spacecraft makes contact with the surface, it must maintain a desired contact force in order to capture a sample. The properties of the surface are unknown or uncertain before contact with the surface is made. Because the nominal robust controller may have poor performance in some surface property regimes, the goal is to improve performance using an adaptive controller. The adaptive controller performs system identification online to create an input–output model of the feedback-linearized system. From the input–output model, a block-observable canonical form is realized and the control input augmentation is determined by model predictive control. The resulting augmentation is added to the input of the robust controller to improve the closed-loop performance and maintain a desired contact force despite the unknown surface properties. The approach is applied to a variety of surface properties with linear and nonlinear contact models and multiple surface sampling maneuvers.

Nomenclature

c_r	=	surface coefficient of restitution
c_s	=	surface damping, N · s/m
e	=	contact force error, N
F_c	=	component of contact force associated with surface compliance, N
F_d	=	desired contact force from surface compliance, N
F_f	=	component of contact force associated with friction, N
$\overline{I}_1, \overline{I}_2$	=	sampling arm intertias, kg/m^2
K	=	robust controller gain
k_s	=	surface stiffness, N/m
L_1, L_2	=	sampling arm length, m
m_s	=	spacecraft sampler mass, kg
m_{sc}	=	spacecraft mass, kg
m_1, m_2	=	sampling arm masses, kg
q	=	spacecraft state
R_1, R_2	=	center of mass location along sampling arm, m
T	=	kinetic energy of spacecraft, J
w_k	=	model coefficients identified by predictive cost adaptive control
x	=	horizontal position of sampler relative to surface, m
y	=	vertical position of sampler relative to surface, m
ζ	=	feedback linearized state
θ_1, θ_2	=	spacecraft sampling arm angles, rad
λ	=	desired exponential decay rate for robust controller
λ_k	=	variable-rate forgetting factor for predictive cost adaptive control
μ	=	surface coefficient of friction
$\tau_{f,k}$	=	discretized feedforward commanded sampler accelerations, m/s^2
τ_1, τ_2	=	sampling arm torques, N · m
$\tau_{1,f}, \tau_{2,f}$	=	feedforward commanded sampler accelerations, m/s^2
χ	=	subblock of feedback linearized state for robust controller

Subscript

k	=	time step for discrete controller

I. Introduction

SURFACE sampling of small celestial bodies has received increasing interest as seen by recent missions such as OSIRIS-REx, Hayabusa, and Hayabusa2. The objective of a sampling mission is to bring a spacecraft with a sampler in contact with the surface of a celestial body and maintain a desired contact force in order to capture a sample from the surface [1,2]. The resulting samples are used to further scientific knowledge about the origins of the solar system and universe.

Despite recent successes, surface sampling remains a challenging problem. Before contact with the surface, surface properties such as the compliance are uncertain. Additional challenges arise due to unknown nonlinear contact dynamics such as hysteretic effects, and the inability to use the spacecraft thrusters to augment the contact force. Therefore, the controller must be designed to be robust to a wide variety of surface properties. If the true surface properties are outside expectations, mission performance will be adversely affected. This was evidenced by the Philae lander, which attempted to land on the comet 67P/Churyumov-Gerasimenko but, due to the surface being softer than expected, instead bounced off of the surface and landed in the shadow of the comet, ending a 10-year-long mission early [3]. Additionally, there is an inherent tradeoff between robustness and control performance, which may limit the possible scope of the mission. As sampling missions become increasingly complex, as shown by sampling mission concepts using shape memory alloy and

Received 1 March 2023; revision received 9 July 2023; accepted for publication 29 July 2023; published online 30 August 2023.

*Ph.D. Candidate, Department of Aerospace Engineering; nmohseni@umich.edu.
†Professor, Department of Aerospace Engineering.
‡Principal Technologist and Group Supervisor, Robotics Modeling and Simulation Group.

harpoon sampling mechanisms, more advanced control algorithms will be needed [4,5].

The challenges associated with surface sampling missions motivate an alternative adaptive approach to the surface sampling control problem. The control algorithm proposed in the present paper consists of a feedback linearization controller with a nominal robust controller that is augmented by an adaptive controller called *predictive cost adaptive control* (PCAC) to adaptively regulate the contact force of the sampler when subject to a surface with unknown properties. The robust controller is developed using a set of linear matrix inequalities (LMIs) to guarantee stability for a wide range of surface properties. The robust controller on its own is unable to meet the performance requirements of the mission, and therefore PCAC is used to augment the commanded sampling arm torques. The present paper proposes an extension of the robust control algorithm given in [6] to the case of an adaptive controller and substantially extends the preliminary results in [7].

PCAC is an adaptive control algorithm that uses a combination of online identification using recursive least squares (RLSs) and model predictive control (MPC) to control uncertain or unknown systems [8,9]. The system identification in PCAC uses an input–output model structure with a variable-rate forgetting (VRF) factor to quickly adjust modeling coefficients when new information is received and to avoid updating modeling coefficients in the presence of noise. The identified model is then transformed into a block-observable canonical form (BOCF) with a known state that can be used by MPC without needing an explicit observer.

The structure of the paper is as follows. Section II describes the spacecraft and contact dynamics of a two-dimensional sampling mission. Section III describes the control architecture for the sampling mission consisting of the feedback linearization controller in Sec. III.A, robust controller in Sec. III.B, and PCAC augmentation in Sec. III.C. Section IV investigates the performance of the proposed algorithm under various surface properties for both linear and nonlinear contact models and a double sampling maneuver scenario.

II. Spacecraft Dynamics and Modeling

An overview of the spacecraft equations of motion and contact dynamics is given in this section. For simplicity, we assume a two-dimensional model, where all masses are rigid. Consider the spacecraft with a two-link sampling arm as shown in Fig. 1. The relative joint angles are given by θ_1 and θ_2; the control torques by τ_1 and τ_2; the spacecraft bus mass by m_{sc}; the link masses and inertias by m_1, m_2, $\bar{I}_1$, and $\bar{I}_2$, respectively; the link lengths and distance to the link center of mass by L_1, L_2, R_1, and R_2, respectively; the sampler position relative to the surface by x and y; and the sampler mass by m_s. The contact and friction forces due to the surface are given by F_c and F_f. Due to the small gravitational forces in this environment, gravitational forces are assumed to be negligible relative to the contact forces and are ignored during the contact phase. The resulting equations of motion have the form

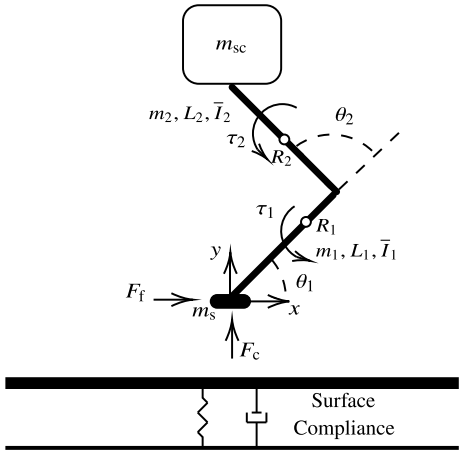

Fig. 1 Spacecraft model for celestial body sampling. Adapted with permission from [7]. Copyright 2022 American Automatic Control Council.

$$M(q)\ddot{q} + D(q,\dot{q})\dot{q} = Q \tag{1}$$

$$q \triangleq \begin{bmatrix} \theta_1 \\ \theta_2 \\ x \\ y \end{bmatrix}, \quad \dot{q} \triangleq \begin{bmatrix} \dot{\theta}_1 \\ \dot{\theta}_2 \\ \dot{x} \\ \dot{y} \end{bmatrix} \tag{2}$$

where $M(q)$, $D(q,\dot{q})$, and Q are the mass, damping, and generalized force matrices. Details of the derivation and structure of these matrices without the sampler mass are given in [6]. The equations of motion for the case where the sampler has mass are derived below.

The position the center of mass of each component of the spacecraft relative to the surface is given by

$$p_s = \begin{bmatrix} x \\ y \end{bmatrix}, \quad p_1 = \begin{bmatrix} x + R_1\cos(\theta_1) \\ y + R_1\sin(\theta_1) \end{bmatrix} \tag{3}$$

$$p_2 = \begin{bmatrix} x + L_1\cos(\theta_1) + R_2\cos(\theta_1+\theta_2) \\ y + L_1\sin(\theta_1) + R_2\sin(\theta_1+\theta_2) \end{bmatrix} \tag{4}$$

$$p_{sc} = \begin{bmatrix} x + L_1\cos(\theta_1) + L_2\cos(\theta_1+\theta_2) \\ y + L_1\sin(\theta_1) + L_2\sin(\theta_1+\theta_2) \end{bmatrix} \tag{5}$$

and velocities by

$$v_s = \begin{bmatrix} \dot{x} \\ \dot{y} \end{bmatrix}, \quad v_1 = \begin{bmatrix} \dot{x} - R_1\dot{\theta}_1\sin(\theta_1) \\ \dot{y} + R_1\dot{\theta}_1\cos(\theta_1) \end{bmatrix} \tag{6}$$

$$v_2 = \begin{bmatrix} \dot{x} - L_1\dot{\theta}_1\sin(\theta_1) - R_2(\dot{\theta}_1+\dot{\theta}_2)\sin(\theta_1+\theta_2) \\ \dot{y} + L_1\dot{\theta}_1\cos(\theta_1) + R_2(\dot{\theta}_1+\dot{\theta}_2)\cos(\theta_1+\theta_2) \end{bmatrix} \tag{7}$$

$$v_{sc} = \begin{bmatrix} \dot{x} - L_1\dot{\theta}_1\sin(\theta_1) - L_2(\dot{\theta}_1+\dot{\theta}_2)\sin(\theta_1+\theta_2) \\ \dot{y} + L_1\dot{\theta}_1\cos(\theta_1) + L_2(\dot{\theta}_1+\dot{\theta}_2)\cos(\theta_1+\theta_2) \end{bmatrix} \tag{8}$$

The velocities and angular velocities of each center of mass can then be written as

$$v_s = A(q)\dot{q} \triangleq \begin{bmatrix} 0 & 0 & 1 & 0 \\ 0 & 0 & 0 & 1 \end{bmatrix}\dot{q} \tag{9}$$

$$v_1 = B(q)\dot{q} \triangleq \begin{bmatrix} -R_1\sin(\theta_1) & 0 & 1 & 0 \\ R_1\cos(\theta_1) & 0 & 0 & 1 \end{bmatrix}\dot{q} \tag{10}$$

$$v_2 = C(q)\dot{q} \triangleq \begin{bmatrix} -L_1\sin(\theta_1) - R_2\sin(\theta_1+\theta_2) & -R_2\sin(\theta_1+\theta_2) & 1 & 0 \\ L_1\cos(\theta_1) + R_2\cos(\theta_1+\theta_2) & R_2\cos(\theta_1+\theta_2) & 0 & 1 \end{bmatrix}\dot{q} \tag{11}$$

$$v_{sc} = D(q)\dot{q} \triangleq \begin{bmatrix} -L_1\sin(\theta_1) - L_2\sin(\theta_1+\theta_2) & -L_2\sin(\theta_1+\theta_2) & 1 & 0 \\ L_1\cos(\theta_1) + L_2\cos(\theta_1+\theta_2) & L_2\cos(\theta_1+\theta_2) & 0 & 1 \end{bmatrix}\dot{q} \tag{12}$$

$$\dot{\theta}_1 = E(q)\dot{q} \triangleq \begin{bmatrix} 1 & 0 & 0 & 0 \end{bmatrix}\dot{q} \tag{13}$$

$$\dot{\theta}_1 + \dot{\theta}_2 = F(q)\dot{q} \triangleq \begin{bmatrix} 1 & 1 & 0 & 0 \end{bmatrix}\dot{q} \tag{14}$$

The kinetic energy T of the spacecraft can then be written as

$$T = \frac{1}{2}\dot{q}^T M(q)\dot{q} \tag{15}$$

where

$$M(q) \triangleq m_s A^T(q)A(q) + m_1 B^T(q)B(q) + m_2 C^T(q)C(q) + m_{sc} D^T(q)D(q) + \bar{I}_1 E^T(q)E(q) + \bar{I}_2 F^T(q)F(q) \tag{16}$$

The following property is given for two matrix functions $A(q)$ and $B(q)$ [10]:

$$\frac{\partial}{\partial q}[A(q)B(q)] \triangleq [I \otimes A(q)]\frac{\partial B(q)}{\partial q} + \frac{\partial A(q)}{\partial q}B(q) \tag{17}$$

where

$$\frac{\partial A(q)}{\partial q} = \begin{bmatrix} \dfrac{\partial A(q)}{\partial q_1} \\ \vdots \\ \dfrac{\partial A(q)}{\partial q_n} \end{bmatrix} \tag{18}$$

The equations of motion are then given by Lagrange's equations

$$\frac{d}{dt}\frac{\partial T}{\partial \dot{q}} - \frac{\partial T}{\partial q} = Q \tag{19}$$

$$M(q)\ddot{q} + \dot{M}(q)\dot{q} - \frac{\partial T}{\partial q} = Q \tag{20}$$

where

$$\dot{M}(q) = \left(\frac{\partial M(q)}{\partial q}\right)^T (\dot{q} \otimes I_4) \tag{21}$$

and using Eq. (17)

$$\frac{\partial T}{\partial q} = \frac{\partial}{\partial q}\left[\frac{1}{2}\dot{q}^T M(q)\dot{q}\right] = \frac{1}{2}\left[I_4 \otimes \dot{q}^T\right]\frac{\partial M(q)}{\partial q}\dot{q} \tag{22}$$

which leads to

$$M(q)\ddot{q} + \left[\left(\frac{\partial M(q)}{\partial q}\right)^T (\dot{q} \otimes I_4) - \frac{1}{2}[I_4 \otimes \dot{q}^T]\frac{\partial M(q)}{\partial q}\right]\dot{q} = Q \tag{23}$$

where

$$\left(\frac{\partial M(q)}{\partial q}\right)^T (\dot{q} \otimes I_4) - \frac{1}{2}\left[I_4 \otimes \dot{q}^T\right]\frac{\partial M(q)}{\partial q} \triangleq D(q, \dot{q}) \tag{24}$$

During contact, the generalized force is given by

$$Q_i = \tau_1 \frac{\partial \dot{\theta}_1}{\partial \dot{q}_i} + \tau_2 \frac{\partial(\dot{\theta}_1 + \dot{\theta}_2)}{\partial \dot{q}_i} + F_f \frac{\partial \dot{x}}{\partial \dot{q}_i} + F_c \frac{\partial \dot{y}}{\partial \dot{q}_i} \quad \text{for } i = 1, 2, 3, 4 \tag{25}$$

$$Q = \begin{bmatrix} 1 & 1 & 0 & 0 \\ 0 & 1 & 0 & 0 \\ 0 & 0 & 1 & 0 \\ 0 & 0 & 0 & 1 \end{bmatrix} \begin{bmatrix} \tau_1 \\ \tau_2 \\ F_f \\ F_c \end{bmatrix} \tag{26}$$

For the contact force, two models commonly used for small celestial body sampling are used. The first is the linear Kelvin–Voigt model [11] given by

$$F_c = -k_s y - c_s \dot{y} \tag{27}$$

where k_s and c_s are the stiffness and damping of the surface material. The second is a nonlinear Hunt–Crossley model [11–13] given by

$$F_c = k_s(-y)^{3/2}\left(1 + \frac{3(1 - c_r)}{2}\frac{\dot{y}}{\dot{y}_0}\right) \tag{28}$$

with coefficient of restitution c_r, surface stiffness k_s, and initial contact velocity $\dot{y}_0$.

Because the contact event occurs with friction, for the friction model, an approximation of the Coulomb force using a regularized friction coefficient is given by

$$F_f \triangleq \begin{cases} -\mu\left(\dfrac{\|\dot{x}\|}{10^{-4}}\right)F_c \operatorname{sgn}(\dot{x}), & 0 \le \dfrac{\|\dot{x}\|}{10^{-4}} \le 1, \\ -\mu F_c \operatorname{sgn}(\dot{x}), & 1 < \dfrac{\|\dot{x}\|}{10^{-4}} \end{cases} \tag{29}$$

where μ is the coefficient of friction [14].

III. Control Architecture

The control architecture for the contact phase is shown in Fig. 2. The controller consists of three components: a feedback linearization controller, a nominal robust controller, and an adaptive controller augmentation using predictive cost adaptive control. The ascent and

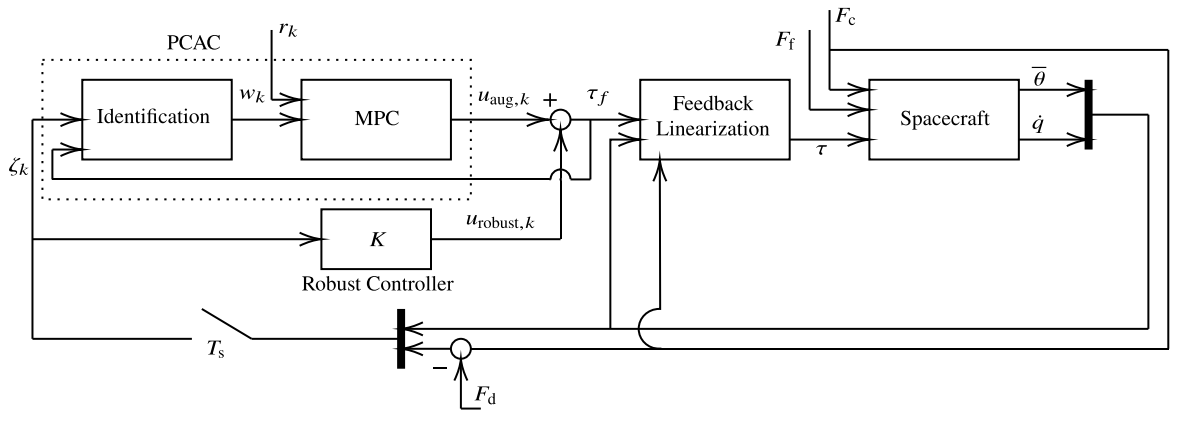

Fig. 2 Adaptive force control architecture for small celestial body sampling.

descent control follows the method given in Ref. [6]. A summary of the control algorithm for the contact phase is given in Algorithm 2.

A. Feedback Linearization Controller

The mass and damping matrices can be decomposed into the following 2×2 partitions:

$$M(q) = \begin{bmatrix} M_1(\bar{\theta}) & M_2(\bar{\theta}) \\ M_2^T(\bar{\theta}) & m_0 I_2 \end{bmatrix},$$
$$D(q,\dot{q}) = \begin{bmatrix} D_1(\bar{\theta},\dot{q}) & D_2(\bar{\theta},\dot{q}) \\ D_2^T(\bar{\theta},\dot{q}) & 0_2 \end{bmatrix}, \quad \bar{\theta} \triangleq \begin{bmatrix} \theta_1 \\ \theta_2 \end{bmatrix} \tag{30}$$

where $m_0 \triangleq m_{sc} + m_1 + m_2 + m_s$. Since $\theta_1, \theta_2, \dot{\theta}_1, \dot{\theta}_2, \dot{x}, \dot{y}$, and F_c are assumed to be measured, the following feedback linearization controller can be used:

$$\begin{bmatrix} \tau_1 \\ \tau_2 \end{bmatrix} = L^{-1}\left[(D_1(\bar{\theta},\dot{q}) - M_1(\bar{\theta})M_2^{-T}(\bar{\theta})D_2^T(\bar{\theta},\dot{q})) \begin{bmatrix} \dot{\theta}_1 \\ \dot{\theta}_2 \end{bmatrix} + D_2(\bar{\theta},\dot{q}) \begin{bmatrix} \dot{x} \\ \dot{y} \end{bmatrix} + M_1(\bar{\theta})M_2^{-T} \begin{bmatrix} 0 \\ 1 \end{bmatrix} F_c + (M_2(\bar{\theta}) - M_1(\bar{\theta})M_2^{-T}(\bar{\theta})m_0 I_2) \begin{bmatrix} \tau_{1,f} \\ \tau_{2,f} \end{bmatrix} \right] \tag{31}$$

where $\tau_{1,f}$ and $\tau_{2,f}$ are the feedforward portion of the feedback linearization controller to be given by a combination of the robust controller (see Sec. III.B) and PCAC (see Sec. III.C), and

$$L \triangleq \begin{bmatrix} 1 & 1 \\ 0 & 1 \end{bmatrix}.$$

For the feedback linearization controller, we assume that the contact force is of the linear form given by Eq. (27). Let the desired contact force be F_d and define the contact force error by

$$e \triangleq F_c - F_d = -k_s y - c_s \dot{y} - F_d \tag{32}$$

Substituting Eq. (31) into Eq. (1) and taking the derivative of Eq. (32) leads to the following dynamics in state-space form:

$$\dot{\zeta} = A(\bar{\theta},\dot{q})\zeta + B(\bar{\theta})\tau_f + E(\bar{\theta})F_f \tag{33}$$

$$\zeta \triangleq \begin{bmatrix} \dot{\theta}_1 \\ \dot{\theta}_2 \\ \dot{x} \\ \dot{y} \\ e \end{bmatrix}, \quad \tau_f \triangleq \begin{bmatrix} \tau_{1,f} \\ \tau_{2,f} \end{bmatrix} \tag{34}$$

$$A(\bar{\theta},\dot{q}) \triangleq \begin{bmatrix} -M_2^{-T}(\bar{\theta})D_2^T(\bar{\theta},\dot{q}) & 0 & 0 & M_2^{-T}(\bar{\theta}) \begin{bmatrix} 0 \\ 1 \end{bmatrix} \\ & 0 & 0 & \\ 0 \quad 0 & 0 & 0 & 0 \\ 0 \quad 0 & 0 & 0 & 0 \\ 0 \quad 0 & 0 & -k_s & 0 \end{bmatrix} \tag{35}$$

$$B(\bar{\theta}) \triangleq \begin{bmatrix} M_2^{-T}(\bar{\theta})m_0 I_2 \\ 1 \quad 0 \\ 0 \quad 1 \\ 0 \quad -c_s \end{bmatrix} \tag{36}$$

$$E(\bar{\theta}) \triangleq \begin{bmatrix} M_2^{-T}(\bar{\theta}) \begin{bmatrix} 1 \\ 0 \end{bmatrix} \\ \xi(\bar{\theta}) \begin{bmatrix} 1 \\ 0 \end{bmatrix} \\ -c_s [0 \quad 1] \xi(\bar{\theta}) \begin{bmatrix} 1 \\ 0 \end{bmatrix} \end{bmatrix} \tag{37}$$

$$\xi(\bar{\theta}) \triangleq (M_2(\bar{\theta}) - M_1(\bar{\theta})M_2^{-T}(\bar{\theta})m_0 I_2)^{-1} M_1(\bar{\theta})M_2^{-T}(\bar{\theta}) \tag{38}$$

B. Robust Controller

We seek to regulate the sampler velocity and error states of Eqs. (35) and (36). It can be seen that the states $\dot{x}$, $\dot{y}$, and e are decoupled from the sampling arm angular rates $\dot{\theta}_1$ and $\dot{\theta}_2$. Therefore, we focus on the block entries of Eqs. (35) and (36) containing the states $\chi = [\dot{x} \quad \dot{y} \quad e]^T$, where

$$\overline{A} \triangleq \begin{bmatrix} 0 & 0 & 0 \\ 0 & 0 & 0 \\ 0 & -k_s & 0 \end{bmatrix}, \quad \overline{B} \triangleq \begin{bmatrix} 1 & 0 \\ 0 & 1 \\ 0 & -c_s \end{bmatrix} \tag{39}$$

The goal is to find a discrete-time controller of the form $\tau_{f,k} = K\chi_k$ that is robust for values of k_s in the range $[k_1, k_2]$ and values of c_s in the range $[c_1, c_2]$. Let $A_{d,i}$ and $B_{d,j}$ be Eq. (39) discretized using a zero-order hold at the sample rate T_s, and stiffness and damping coefficients k_i and c_j. The control gain K that exponentially stabilizes the system for the range of stiffness and damping coefficients must satisfy the following set of Lyapunov equations:

$$(A_{d,i} + B_{d,j}K)Q(A_{d,i} + B_{d,j}K)^T - e^{-2\lambda T_s}Q \le 0 \quad \text{for } i = 1,2 \text{ and } j = 1,2, \quad Q > 0 \tag{40}$$

where Q is a positive-definite matrix, and λ is a tuning parameter representing the slowest desired exponential decay rate of the closed-loop system for all combinations of stiffness and damping parameters in the range $[k_1, k_2]$ and $[c_1, c_2]$ [15]. Using the Schur complement, defining $Y \triangleq KQ$, and incorporating a slack variable s, Eq. (40) can be rewritten as a set of LMI constraints in the following optimization problem:

$$\begin{aligned} \min_{Q,Y} \quad & s \\ \text{s.t.} \quad & \begin{bmatrix} e^{-2\lambda T_s}Q & (A_{d,i}Q + B_{d,j}Y) \\ (A_{d,i}Q + B_{d,j}Y)^T & Q \end{bmatrix} \ge \begin{bmatrix} sI_3 & 0_3 \\ 0_3 & 0_3 \end{bmatrix} \\ & \text{for } i = 1,2 \text{ and } j = 1,2, \\ & Q \ge sI_3 \\ & s \ge 0 \end{aligned} \tag{41}$$

which can be solved using CVX [16,17]. The resulting robust controller is then given by $K = YQ^{-1}$.

C. Predictive Cost Adaptive Control

PCAC combines online identification using RLSs with a forgetting factor, and a model predictive controller in two separate steps [8]. For the purposes of augmenting the nominal robust controller for surface sampling, the identification portion attempts to identify the feedback-linearized system without the robust controller. The identified model is then augmented with the robust controller and sent to the MPC portion of PCAC. The MPC controller outputs a torque augmentation that is added to the torque command produced by the robust controller.

1. Online Identification

Consider the multi–input multi–output input–output model

$$\hat{y}_k = -\sum_{i=1}^{\hat{n}} \hat{F}_i y_{k-i} + \sum_{i=1}^{\hat{n}} \hat{G}_i \tau_{f,k-i} \tag{42}$$

where $k \geq 0$ is the time step, $\hat{n} \geq 1$ is the identification data window, $\hat{F}_i \in \mathbb{R}^{p\times p}$ and $\hat{G}_i \in \mathbb{R}^{p\times m}$ are the estimated model coefficients, and $\tau_{f,k} \in \mathbb{R}^{m\times 1}$, $y_k \in \mathbb{R}^{p\times 1}$, and $\hat{y}_k \in \mathbb{R}^{p\times 1}$ are the inputs, outputs, and predicted outputs at step k, respectively.

To estimate the coefficients $\hat{F}_i$ and $\hat{G}_i$ online, we use RLSs with VRF [18]. RLSs minimize the cumulative cost

$$J_k(\hat{w}) = \sum_{i=0}^{k} \frac{\rho_i}{\rho_k} z_i^T(\hat{w}) z_i(\hat{w}) + \frac{1}{\rho_k}(\hat{w} - w_0)^T P_0^{-1}(\hat{w} - w_0) \tag{43}$$

where $\rho_k \triangleq \prod_{j=0}^{k} \lambda_j^{-1} \in \mathbb{R}$, $\lambda_k \in (0, 1]$ is the forgetting factor, $P_0 \in \mathbb{R}^{[\hat{n}p(m+p)]\times[\hat{n}p(m+p)]}$ is positive definite, and $w_0 \in \mathbb{R}^{[\hat{n}p(m+p)]\times 1}$ is the initial estimate of the coefficient vector. The performance variable $z_i(\hat{w}) \in \mathbb{R}^{p\times 1}$ is defined as

$$z_k(\hat{w}) \triangleq y_k + \sum_{i=1}^{\hat{n}} \hat{F}_i y_{k-i} - \sum_{i=1}^{\hat{n}} \hat{G}_i \tau_{f,k-i} \tag{44}$$

where the vector $\hat{w} \in \mathbb{R}^{[\hat{n}p(m+p)]\times 1}$ of coefficients to be estimated is defined by

$$\hat{w} \triangleq \mathrm{vec}\begin{bmatrix} \hat{F}_1 & \cdots & \hat{F}_{\hat{n}} & \hat{G}_1 & \cdots & \hat{G}_{\hat{n}} \end{bmatrix} \tag{45}$$

Defining the regressor matrix $\phi_k \in \mathbb{R}^{p\times[\hat{n}p(m+p)]}$ by

$$\phi_k \triangleq \begin{bmatrix} -y_{k-1}^T & \cdots & -y_{k-\hat{n}}^T & \tau_{f,k-1}^T & \cdots & \tau_{f,k-\hat{n}}^T \end{bmatrix} \otimes I_p \tag{46}$$

the performance variable can be written as

$$z_k(\hat{w}) = y_k - \phi_k \hat{w} \tag{47}$$

The global minimizer $w_{k+1} \triangleq \mathrm{argmin}_{\hat{w}} J_k(\hat{w})$ is computed by RLSs as

$$P_{k+1} = \lambda_k^{-1} P_k - \lambda_k^{-1} P_k \phi_k^T (\lambda_k I_p + \phi_k P_k \phi_k^T)^{-1} \phi_k P_k \tag{48}$$

$$w_{k+1} = w_k + P_{k+1} \phi_k^T (y_k - \phi_k \hat{w}) \tag{49}$$

where $w_{k+1} = \mathrm{vec}[\, \hat{F}_{1,k+1} \ \cdots \ \hat{F}_{\hat{n},k+1} \quad \hat{G}_{1,k+1} \ \cdots \ \hat{G}_{\hat{n},k+1}\,]$.

The VRF factor λ_k is developed in [19] and given by

$$\lambda_k = \frac{1}{1 + \eta g(z_{k-\tau_d}, \ldots, z_k) \mathbf{1}[g(z_{k-\tau_d}, \ldots, z_k)]} \tag{50}$$

where $\mathbf{1}: \mathbb{R} \to \{0, 1\}$ is the unit step function, and

$$g(z_{k-\tau_d}, \ldots, z_k) \triangleq \sqrt{\frac{\tau_n}{\tau_d} \frac{\mathrm{tr}(\Sigma_{\tau_n}(z_{k-\tau_n}, \ldots, z_k)\Sigma_{\tau_d}(z_{k-\tau_d}, \ldots, z_k)^{-1})}{c}} - \sqrt{f} \tag{51}$$

where $\eta > 0$ and $p \leq \tau_n < \tau_d$ represent numerator and denominator window lengths, respectively. In Eq. (51), Σ_{τ_n} and $\Sigma_{\tau_d} \in \mathbb{R}^{p\times p}$ are the sample variances of the respective window lengths, c is a constant given by

$$a \triangleq \frac{(\tau_n + \tau_d - p - 1)(\tau_d - 1)}{(\tau_d - p - 3)(\tau_d - p)}, \quad b \triangleq 4 + \frac{(p\tau_n + 2)}{(a - 1)},$$
$$c \triangleq \frac{p\tau_n(b - 2)}{b(\tau_d - p - 1)} \tag{52}$$

$f \triangleq F^{-1}_{p\tau_n,b}(1 - \alpha)$ is a thresholding constant, where $F^{-1}_{p\tau_n,b}(x)$ is the inverse cumulative distribution function of the F-distribution with degrees of freedom $p\tau_n$ and b, and α is the significance level [20].

For MPC, the input–output model (42) is written as the BOCF state-space realization augmented by the robust controller

$$x_{1|k} \triangleq \hat{A}_k \hat{x}_k + \hat{B}_k u_{\mathrm{aug},k},$$
$$y_k = \hat{C} \hat{x}_k \tag{53}$$

where $x_{1|k} \in \mathbb{R}^{\hat{n}p}$ is the one-step predicted state, $\hat{x}_k \triangleq \begin{bmatrix} \hat{x}_{1,k}^T & \cdots & \hat{x}_{\hat{n},k}^T \end{bmatrix}^T \in \mathbb{R}^{\hat{n}p}$ is the state estimate, and

$$\hat{x}_{1,k} \triangleq y_k \tag{54}$$

$$\hat{x}_{i,k} \triangleq -\sum_{j=1}^{\hat{n}-i+1} \hat{F}_{i+j-1,k+1} y_{k-j} + \sum_{j=1}^{\hat{n}-i+1} \hat{G}_{i+j-1,k+1} \tau_{f,k-j}, \quad i = 2, \ldots, \hat{n} \tag{55}$$

$$\hat{A}_k \triangleq \begin{bmatrix} -\hat{F}_{1,k+1} & I_p & \cdots & \cdots & 0_{p\times p} \\ \vdots & 0_{p\times p} & \ddots & & \vdots \\ \vdots & \vdots & \ddots & \ddots & 0_{p\times p} \\ \vdots & \vdots & & \ddots & I_p \\ -\hat{F}_{\hat{n},k+1} & 0_{p\times p} & \cdots & \cdots & 0_{p\times p} \end{bmatrix} + \begin{bmatrix} \hat{G}_{1,k+1} \\ \hat{G}_{2,k+1} \\ \vdots \\ \hat{G}_{\hat{n},k+1} \end{bmatrix} K \tag{56}$$

$$\hat{B}_k \triangleq \begin{bmatrix} \hat{G}_{1,k+1} \\ \hat{G}_{2,k+1} \\ \vdots \\ \hat{G}_{\hat{n},k+1} \end{bmatrix}, \quad \hat{C} \triangleq \begin{bmatrix} I_p & 0_{p\times p} & \cdots & 0_{p\times p} \end{bmatrix} \tag{57}$$

2. Model Predictive Control

The ℓ-step predicted output of Eq. (53) for a sequence of ℓ future controls is given by

$$Y_{1|k,l} = \hat{\Gamma}_{k,\ell} x_{1|k} + \hat{T}_{k,\ell} U_{1|k,\ell} \tag{58}$$

where

$$Y_{1|k,\ell} \triangleq \begin{bmatrix} y_{1|k} \\ \vdots \\ y_{\ell|k} \end{bmatrix} \in \mathbb{R}^{\ell p}, \quad U_{1|k,\ell} \triangleq \begin{bmatrix} u_{1|k} \\ \vdots \\ u_{\ell|k} \end{bmatrix} \in \mathbb{R}^{\ell m} \tag{59}$$

and $\hat{\Gamma}_{k,\ell} \in \mathbb{R}^{\ell p\times \hat{n}p}$ and $\hat{T}_{k,\ell} \in \mathbb{R}^{\ell p\times \ell m}$ are

$$\hat{\Gamma}_{k,\ell} \triangleq \begin{bmatrix} \hat{C} \\ \hat{C}\hat{A}_k \\ \vdots \\ \hat{C}\hat{A}_k^{\ell-1} \end{bmatrix}, \quad \hat{T}_{k,\ell} \triangleq \begin{bmatrix} 0_{p\times m} & \cdots & \cdots & \cdots & 0_{p\times m} \\ \hat{H}_{k,1} & 0_{p\times m} & \cdots & \cdots & 0_{p\times m} \\ \hat{H}_{k,2} & \hat{H}_{k,1} & \ddots & \cdots & 0_{p\times m} \\ \vdots & \vdots & \ddots & \ddots & \vdots \\ \hat{H}_{k,\ell-1} & \hat{H}_{k,\ell-2} & \cdots & \hat{H}_{k,1} & 0_{p\times m} \end{bmatrix}$$

where $\hat{H}_{k,i} \in \mathbb{R}^{p\times m}$ is defined by $\hat{H}_{k,i} \triangleq \hat{C}\hat{A}_k^{i-1}\hat{B}_k$.

Let $\mathcal{R}_{k,\ell} \triangleq [\, r_{k+1}^T \ \cdots \ r_{k+\ell}^T \,]^T \in \mathbb{R}^{\ell p_t}$ be the vector of ℓ future commands, $C_{t,\ell} \triangleq I_\ell \otimes C_t \in \mathbb{R}^{\ell p_t \times \ell p}$, where $C_t y_{i|k}$ creates the tracking outputs from $y_{i|k}$; let $Y_{t,1|k,\ell} \triangleq C_{t,\ell} Y_{1|k,\ell}$ be the ℓ-step predicted tracking output; and define $\Delta U_{1|k,\ell} \in \mathbb{R}^{\ell m\times 1}$ as

$$\Delta U_{1|k,\ell} \triangleq \begin{bmatrix} (u_{1|k} - u_k)^T & \cdots & (u_{\ell|k} - u_{\ell-1|k})^T \end{bmatrix}^T \tag{60}$$

The receding horizon optimization problem is then given by

$$\begin{aligned} &\min_{U_{1|k,\ell}} \ (Y_{t,1|k,\ell} - \mathcal{R}_{k,\ell})^T Q (Y_{t,1|k,\ell} - \mathcal{R}_{k,\ell}) + \Delta U_{1|k,\ell}^T R \Delta U_{1|k,\ell} \\ &\text{s.t. } U_{\min} \le U_{1|k,\ell} \le U_{\max} \\ &\qquad \Delta U_{\min} \le \Delta U_{1|k,\ell} \le \Delta U_{\max} \end{aligned} \tag{61}$$

where $Q \in \mathbb{R}^{\ell p_t \times \ell p_t}$ is the positive-definite tracking weight, $R \in \mathbb{R}^{\ell m\times \ell m}$ is the positive-definite control move-size weight, $U_{\min} \triangleq 1_{\ell\times 1} \otimes u_{\min} \in \mathbb{R}^{\ell m}$, $U_{\max} \triangleq 1_{\ell\times 1} \otimes u_{\max} \in \mathbb{R}^{\ell m}$, $\Delta U_{\min} \triangleq 1_{\ell\times 1} \otimes \Delta u_{\min} \in \mathbb{R}^{\ell m}$, and $\Delta U_{\max} \triangleq 1_{\ell\times 1} \otimes \Delta u_{\max} \in \mathbb{R}^{\ell m}$. The first entry of $U_{1|k,\ell}$ is then used as the control augmentation $u_{\text{aug},k}$.

IV. Examples

To demonstrate the advantage of the adaptive augmentation method, we compare the algorithm to the nominal robust controller for a variety of surface properties, including linear and nonlinear contact models. We also demonstrate a double sampling maneuver where the sampler mass increases by an unknown amount after obtaining a surface sample from the first maneuver before descending onto the surface again to obtain additional material. In these examples, the spacecraft in Fig. 1 descends onto the surface at a speed of 0.1 m/s starting from a height of 0.2 m. There are seven sensors measuring θ_1, θ_2, $\dot{\theta}_1$, $\dot{\theta}_2$, $\dot{x}$, $\dot{y}$, and F_c. Once contact is made, the controller attempts to regulate the sampler's contact force to $F_d = 25$ N and its x and y velocity to 0 before departing the surface after 2 s.

Algorithm 1: PCAC identification

Initialize: $\hat{w}_0 \in \mathbb{R}^{[\hat{n}p(m+p)]\times 1}$, $P_0 \in \mathbb{R}^{[\hat{n}p(m+p)]\times[\hat{n}p(m+p)]}$ positive definite, $\tau_d > \tau_n \ge p$, $\eta > 0$, $\alpha > 0$, $k = 0$, and a buffer of $\tau_d + 1$ previous performance variables initialized as 0

function PCAC_ID $y_k, \tau_{f,k}$

$z_k \leftarrow y_k - \phi_k \hat{w}_k$

Add z_k to performance variable buffer and remove oldest entry

Compute sample covariance matrices $\Sigma_{\tau_n} \in \mathbb{R}^{p\times p}$ and $\Sigma_{\tau_d} \in \mathbb{R}^{p\times p}$ from previous $\tau_n + 1$ and $\tau_d + 1$ errors from buffer

if $k \ge \tau_d + 1$ **then**

Compute a, b, and c using Eq. (52)

$g \leftarrow$ Eq. (51)

else

$g \leftarrow 0$

end if

$\beta_k \leftarrow 1 + \eta g \mathbf{1}[g]$

$L_k \leftarrow \beta_k P_k$

$w_{k+1} \leftarrow w_k + P_{k+1}\phi_k^T (y_k - \phi_k w_k)$

$P_{k+1} \leftarrow L_k - L_k \phi_k^T (I_p + \phi_k L_k \phi_k^T)^{-1} \phi_k L_k$

$\phi_{k+1} \leftarrow$ Update regressor ϕ_k with current measurement and input

end function

Algorithm 2: Adaptive force control augmentation

Initialize: $p = 5$, $m = 2$, Sample rate T_s, Solve Eq. (41) to get K, $\tau_{f,0} = 0_{m\times 1}$, $k = 0$

while In contact phase **do**

Measure $\theta_1, \theta_2, \zeta_k = [\, \dot{\theta}_1 \quad \dot{\theta}_2 \quad \dot{x} \quad \dot{y} \quad e \,]^T \in \mathbb{R}^{p\times 1}$, and $\chi_k = [\, \dot{x} \quad \dot{y} \quad e \,]^T \in \mathbb{R}^{p-2\times 1}$

Start Robust Controller

$u_{\text{robust},k} \leftarrow K\chi_k$

End Robust Controller

Start PCAC Identification

$y_k \leftarrow \zeta_k$ State measurement

$w_{k+1} \leftarrow$ PCAC_ID$(y_k, \tau_{f,k})$

End PCAC Identification

$\hat{x}_k \leftarrow w_{k+1}, y_k$ from Eqs. (54) and (55)

$K \leftarrow [\, 0_2 \quad K \,]$

$\hat{A}_k, \hat{B}_k, \hat{C} \leftarrow w_{k+1}, K$ from Eqs. (56) and (57)

Start PCAC MPC

$U_{1|k,\ell} \leftarrow$ Solve Eq. (61)

$u_{\text{aug},k} \leftarrow [\, I_m \quad 0_{m\times(\ell-1)m} \,] U_{1|k,\ell}$

End PCAC MPC

$\tau_{f,k} \leftarrow u_{\text{robust},k} + u_{\text{aug},k}$

Start Feedback Linearization

$\tau_f \leftarrow \tau_{f,k}$

$[\, \tau_1 \quad \tau_2 \,]^T \leftarrow \tau_f$ from Eq. (31)

End Feedback Linearization

$k \leftarrow k + 1$

end while

The spacecraft parameters are $m_{\text{sc}} = 420$ kg, $m_1 = m_2 = m_s = 1$ kg, $L_1 = L_2 = 2$ m, $R_1 = R_2 = 1$ m, $\overline{I}_1 = \overline{I}_2 = (1/3)$ kg/m^2, $\theta_{1,0} = \pi/4$, and $\theta_{2,0} = \pi/2$. The surface coefficient of friction is taken to be $\mu = 0.5$. The robust controller parameters were taken to be $\lambda = 0.05$, $k_1 = 300$ N/m, $k_2 = 2.7 \times 10^5$ N/m, $c_1 = 0.35$ N $\cdot$ s/m, and $c_2 = 10^3$ N $\cdot$ s/m. PCAC is initialized with $p = 5$, $m = 2$, $\hat{n} = 1$, $P_0 = 10 I_{35}$, $\eta = 0.1$, $\tau_n = 40$, $\tau_d = 200$, $\alpha = 0.001$, $\ell = 50$, $Q = I_\ell \otimes \text{diag}(1000, 100, 1)$, $R = 1 I_{\ell m}$, $C_t = [0_{3\times 2} \ I_3]$, $u_{\max} = -u_{\min} = 100$, and $\mathcal{R}_{k,\ell} = 1_{3\times\ell} \otimes [0 \ 0 \ 0]^T$. The initial PCAC model coefficients w_0 are initialized to match the zero-order-hold discretized model of Eqs. (35) and (36), with the linear surface contact model $k_s = 100$ N/m and $c_s = 10^3$ N $\cdot$ s/m, and $\overline{\theta}$ and $\dot{q}$ being set to their respective values at contact. This makes w_0 a 35-parameter vector. The controller runs in a sample-data feedback loop at 2 kHz.

A. Linear Contact Model

Assuming that the surface has the linear Kelvin–Voigt contact model (27), we compare the performance of the robust controller and augmented robust controller with PCAC for stiffness coefficients between 300 and 2.7×10^5 N/m, and damping coefficients 0.35 and 10^3 N $\cdot$ s/m. Figure 3 shows the median contact force over the 2 s contact period over the range of surface properties. Notice that the nominal robust controller has difficulty reaching the desired contact force for low surface stiffness coefficients, while the augmented controller consistently reaches the desired contact force for all tested surface properties. Figure 4 shows the contact force, sampler velocity, actuator torques, and PCAC model coefficients for the surface properties $k_s = 2 \times 10^5$ and $c_s = 5$ N $\cdot$ s/m. Notice that the PCAC-augmented controller quickly reaches the desired contact force, while the nominal robust controller on its own takes most of the 2 s contact period to reach the desired contact force of 25 N.

B. Nonlinear Contact Model

Assuming that the surface has the nonlinear Hunt–Crossley contact model (28), we compare the performance of the robust controller and augmented robust controller with PCAC for stiffness coefficients between 300 and 2.7×10^5 N/m, and coefficient of restitution between 0.1 and 1. Figure 5 shows the median contact force over

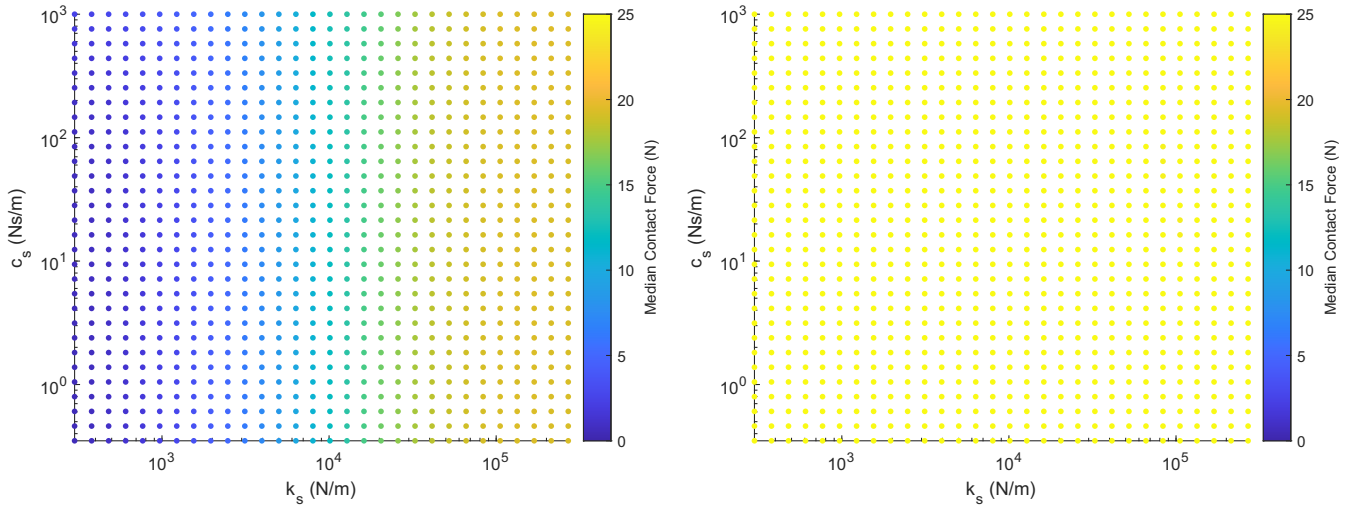

a) Robust controller b) PCAC augmented controller

Fig. 3 Median contact force for various surface stiffness k_s and damping c_s values using the linear Kelvin–Voigt contact model (27).

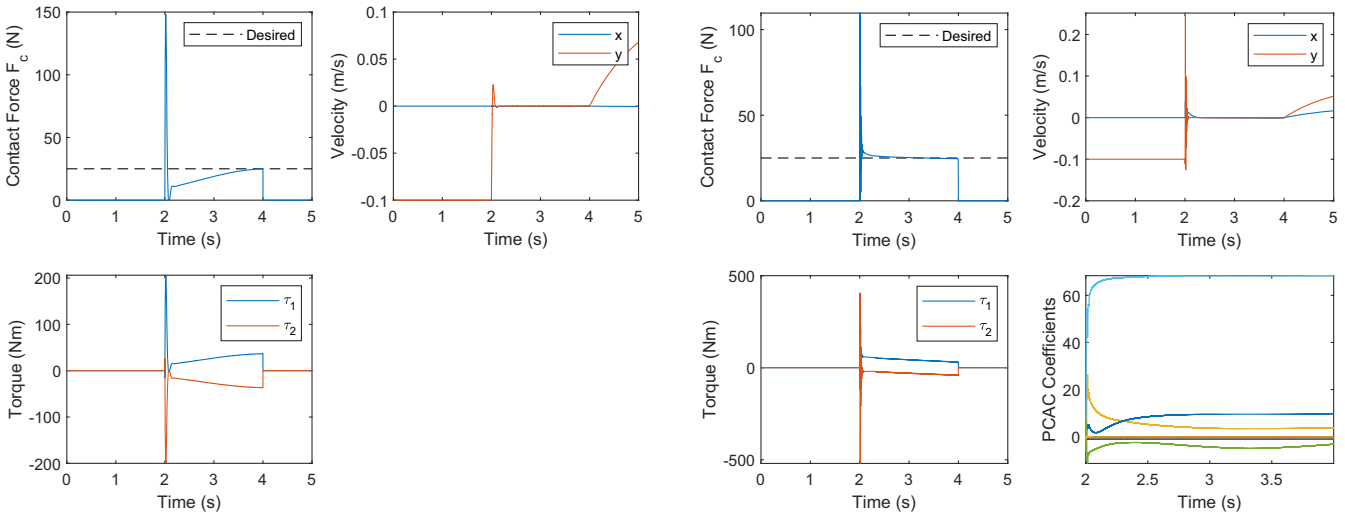

a) Robust controller b) PCAC augmented controller

Fig. 4 Contact force, sampler velocity, actuator torques, and PCAC model coefficients for the linear contact model (27) with $k_s = 2 \times 10^5$ N/m and $c_s = 5$ N · s/m.

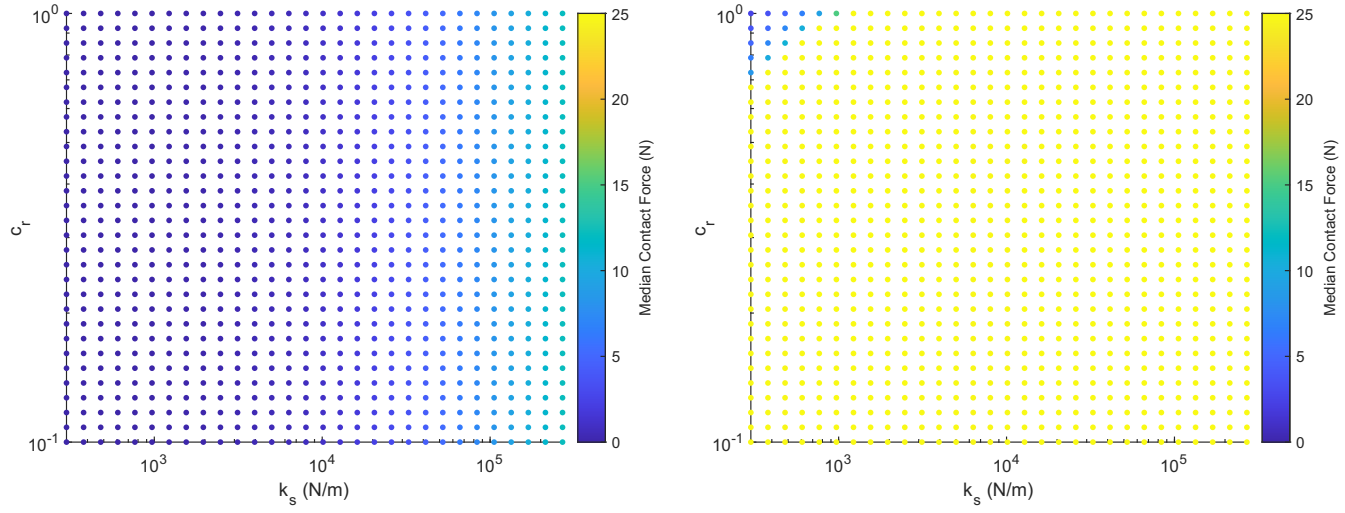

a) Robust controller b) PCAC augmented controller

Fig. 5 Median contact force for various surface stiffness k_s and damping c_s values using the nonlinear Hunt–Crossley contact model (28).

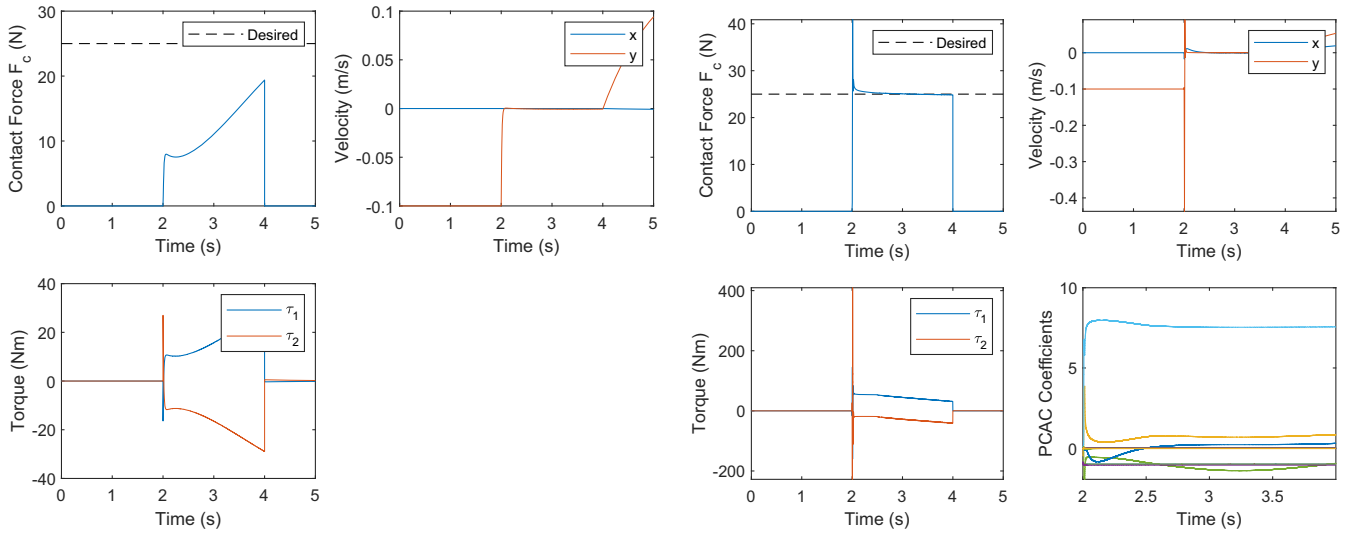

a) Robust controller **b) PCAC augmented controller**

Fig. 6 Contact force, sampler velocity, actuator torques, and PCAC model coefficients for the nonlinear contact model (28) with $k_s = 2 \times 10^5$ N/m and $c_r = 0.9$.

the 2 s contact period over the range of surface properties. Notice that the nominal robust controller's median contact force has difficulty reaching even half of the desired 25 N, while the augmented controller consistently reaches the desired contact force for all tested surface properties except for situations where there is low stiffness combined with a high coefficient of restitution. Figure 6 shows the contact force, sampler velocity, actuator torques, and PCAC model coefficients for the surface properties $k_s = 2 \times 10^5$ N/m and $c_r = 0.9$. Notice that the PCAC-augmented controller quickly reaches the desired contact force while the nominal robust controller never does.

C. Double Sampling Maneuver with Linear Contact Model

We now consider a double sampling maneuver where after descending onto the surface and collecting a sample, the spacecraft then descends again onto a different region of the celestial body to collect additional material. The amount of material collected on the first maneuver is chosen to be 0.5 kg and is unknown to the spacecraft. Assuming that the surface has the linear Kelvin–Voigt contact model (27), the surface on the first maneuver has properties $k_s = 2 \times 10^5$ N/m and $c_s = 5$ N · s/m, and the surface on the second maneuver has $k_s = 200$ N/m and $c_s = 500$ N · s/m. Figure 7 shows that the desired contact force is reached for both maneuvers. Notice that on contact with the new surface at 8 s, the RLS VRF factor λ_k automatically decreases, enabling forgetting of the old surface properties and causing an increase in the trace of the RLS covariance $\mathrm{tr}(P_k)$ to allow for fast identification of a new surface contact model.

D. Double Sampling Maneuver with Nonlinear Contact Model

For the double sampling maneuver, assuming that the surface has the nonlinear Hunt–Crossley contact model (28), the surface on the first maneuver has properties $k_s = 2 \times 10^5$ N/m and $c_r = 0.9$, and the surface on the second maneuver has $k_s = 300$ N/m and $c_r = 0.2$. Figure 8 shows that the desired contact force is reached for both maneuvers. Notice that on contact with the new surface at 8 s the RLS VRF factor λ_k automatically decreases, enabling forgetting of

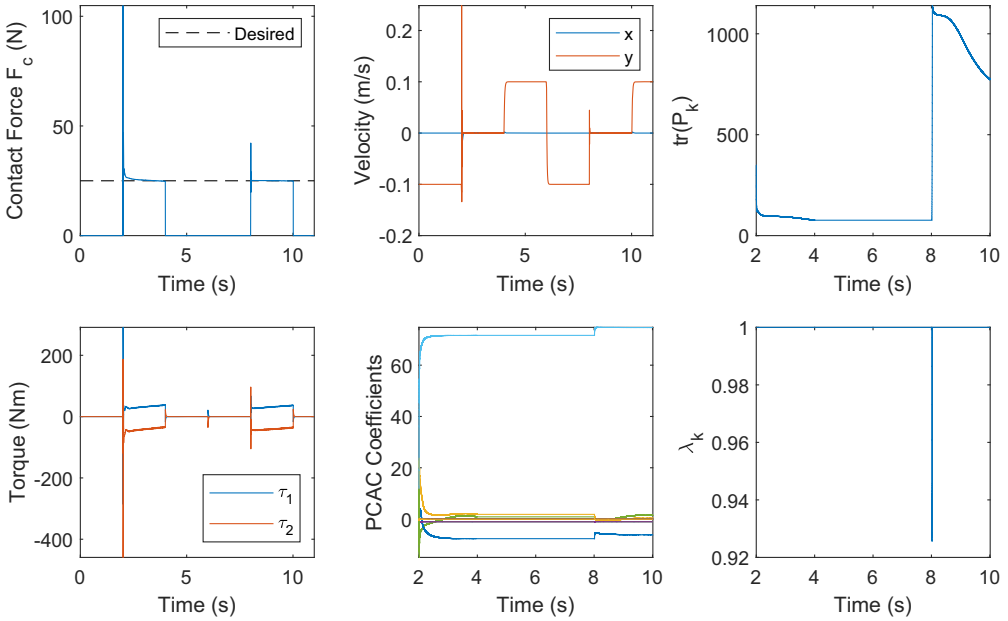

Fig. 7 Contact force, sampler velocity, actuator torques, and PCAC model coefficients for a double sampling maneuver with the linear contact model (27) with $k_s = 2 \times 10^5$ N/m and $c_s = 5$ N · s/m for the first maneuver and $k_s = 200$ N/m and $c_s = 500$ N · s/m for the second maneuver.

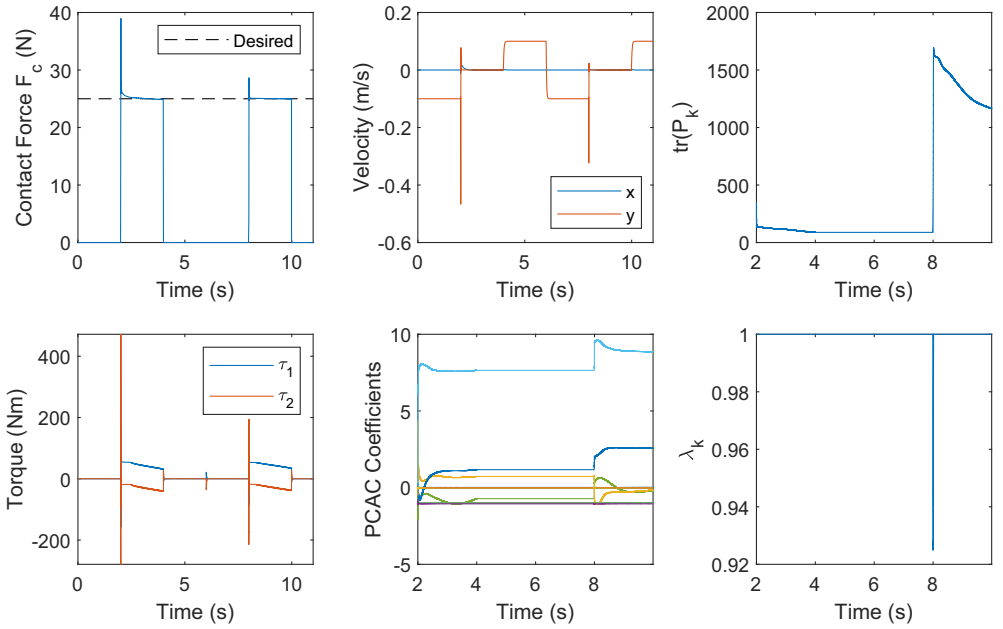

Fig. 8 Contact force, sampler velocity, actuator torques, and PCAC model coefficients for a double sampling maneuver with the nonlinear contact model (28) with $k_s = 2 \times 10^5$ N/m and $c_r = 0.9$ for the first maneuver, and $k_s = 300$ N/m and $c_r = 0.2$ for the second maneuver.

the old surface properties and causing an increase in the trace of the RLS covariance $\mathrm{tr}(P_k)$ to allow for fast identification of a new surface contact model.

V. Conclusions

This paper developed and investigated the performance of an adaptive force control augmentation algorithm for spacecraft sampling maneuvers on small celestial bodies. The algorithm consisted of a nominal robust controller with an adaptive augmentation using PCAC combined with feedback linearization to maintain a desired contact force during the sampling maneuver. PCAC uses output-feedback MPC without an estimator and with concurrent online identification. Both linear and nonlinear contact models were used to investigate the controller's performance under various surface properties. Additionally, a double sampling maneuver was investigated where the spacecraft collected an unknown amount of material from an initial maneuver before ascending and descending and then sampling from a different region of the celestial body with different surface properties. The controller was shown to reach the desired contact force over a wide range of surface properties and outperformed the nominal robust controller in all cases. For the double sampling maneuver, PCAC was able to identify a new model of the surface and successfully adjust the control input to reach the desired contact force on the second surface.

When contact is first made with the surface, there is an initially large transient force exerted on the sampler. This can be mitigated using a combination of the proposed control algorithm and passive damping of the sampling arm. The inclusion of passive damping lessens the total required control input. Additionally, investigation of more accurate surface contact models is of interest. Complementarity contact models and high-fidelity, particle-based soil-contact models are possible avenues for improving the simulation accuracy of the sampling maneuver.

Acknowledgments

This work was supported by NASA Space Technology Graduate Research Opportunity under grant number 80NSSC20K1164. Quadrelli's contribution was carried out at the Jet Propulsion Laboratory, California Institute of Technology, under a contract with NASA.

References

[1] May, A., Sutter, B., Linn, T., Bierhaus, B., Berry, K., and Mink, R., "OSIRIS-REx Touch-and-Go (TAG) Mission Design for Asteroid Sample Collection," *International Astronautical Congress*, Vol. 65, International Astronautical Federation, Paris, France, 2014, pp. 1–11.

[2] Ajluni, T., Everett, D., Linn, T., Mink, R., Willcockson, W., and Wood, J., "OSIRIS-REx, Returning the Asteroid Sample," *2015 IEEE Aerospace Conference*, IEEE, New York, 2015, pp. 1–15. https://doi.org/10.1109/AERO.2015.7118988

[3] Biele, J., Ulamec, S., Maibaum, M., Roll, R., Witte, L., Jurado, E., Muñoz, P., Arnold, W., Auster, H. U., Casas, C., and Faber, C., "The Landing(s) of Philae and Inferences About Comet Surface Mechanical Properties," *Science*, Vol. 349, No. 6247, 2015, pp. 1–6. https://doi.org/10.1126/science.aaa9816

[4] Quadrelli, M. B., Backes, P., Wilkie, W. K., Giersch, L., Quijano, U., Keim, J., Scharf, D., Mukherjee, R., Bradford, S. C., and McKee, M., "Investigation of Phase Transition-Based Tethered Systems for Small Body Sample Capture," *Acta Astronautica*, Vol. 68, No. 7, 2011, pp. 947–973. https://doi.org/10.1016/j.actaastro.2010.08.040

[5] Quadrelli, M. B., Ono, M., and Jain, A., "Modeling of Active Tether System Concepts for Planetary Exploration," *Acta Astronautica*, Vol. 138, Sept. 2017, pp. 512–529. https://doi.org/10.1016/j.actaastro.2016.11.010

[6] Acikmese, B., Quadrelli, M., and Phan, L., "A Force Control Algorithm for Small Celestial Body Surface Sampling," *AIAA Guidance, Navigation and Control Conference and Exhibit*, AIAA Paper 2007-6322, 2007. https://doi.org/10.2514/6.2007-6322

[7] Mohseni, N., Bernstein, D. S., and Quadrelli, M. B., "Adaptive Force Control for Small Celestial Body Sampling," *2022 American Control Conference (ACC)*, IEEE, New York, 2022, pp. 2515–2520. https://doi.org/10.23919/ACC53348.2022.9867531

[8] Nguyen, T., Islam, S. A. U., Bernstein, D. S., and Kolmanovsky, I., "Predictive Cost Adaptive Control: A Numerical Investigation of Persistency, Consistency, and Exigency," *IEEE Control Systems Magazine*, Vol. 41, No. 6, 2021, pp. 64–96. https://doi.org/10.1109/MCS.2021.3107647

[9] Mohseni, N., Nguyen, T. W., Ul Islam, S. A., Kolmanovsky, I. V., and Bernstein, D. S., "Active Noise Control for Harmonic and Broadband Disturbances Using RLS-Based Model Predictive Control," *2020 American Control Conference (ACC)*, IEEE, New York, 2020, pp. 1393–1398. https://doi.org/10.23919/ACC45564.2020.9147440

[10] Brewer, J., "Kronecker Products and Matrix Calculus in System Theory," *IEEE Transactions on Circuits and Systems*, Vol. 25, No. 9, 1978, pp. 772–781. https://doi.org/10.1109/TCS.1978.1084534

[11] Flores, P., "Compliant Contact Force Approach for Forward Dynamic Modeling and Analysis of Biomechanical Systems," *Procedia IUTAM*, Vol. 2, Elsevier, New York, 2011, pp. 58–67. https://doi.org/10.1016/j.piutam.2011.04.006

[12] Hunt, K. H., and Crossley, F. R. E., "Coefficient of Restitution Interpreted as Damping in Vibroimpact," *Journal of Applied Mechanics*, Vol. 42, No. 2, 1975, pp. 440–445. https://doi.org/10.1115/1.3423596

[13] Schwartz, S. R., Michel, P., Richardson, D. C., and Yano, H., "Low-Speed Impact Simulations into Regolith in Support of Asteroid Sampling Mechanism Design I: Comparison with 1-g Experiments," *Planetary and Space Science*, Vol. 103, Nov. 2014, pp. 174–183. https://doi.org/10.1016/j.pss.2014.07.013

[14] Castro, A. M., Qu, A., Kuppuswamy, N., Alspach, A., and Sherman, M., "A Transition-Aware Method for the Simulation of Compliant Contact with Regularized Friction," *IEEE Robotics and Automation Letters*, Vol. 5, No. 2, 2020, pp. 1859–1866. https://doi.org/10.1109/LRA.2020.2969933

[15] Boyd, S., El Ghaoui, L., Feron, E., and Balakrishnan, V., *Linear Matrix Inequalities in System and Control Theory*, Soc. for Industrial and Applied Mathematics, Philadelphia, PA, 1994, Chap. 7. https://doi.org/10.1137/1.9781611970777

[16] Grant, M., and Boyd, S., "CVX: Matlab Software for Disciplined Convex Programming, Version 2.1," March 2014, http://cvxr.com/cvx.

[17] Grant, M., and Boyd, S., "Graph Implementations for Nonsmooth Convex Programs," *Recent Advances in Learning and Control*, edited by V. Blondel, S. Boyd, and H. Kimura, Lecture Notes in Control and Information Sciences, Springer–Verlag, Berlin, 2008, pp. 95–110. https://doi.org/10.1007/978-1-84800-155-8_7

[18] Bruce, A. L., Goel, A., and Bernstein, D. S., "Convergence and Consistency of Recursive Least Squares with Variable-Rate Forgetting," *Automatica*, Vol. 119, Sept. 2020, Paper 109052. https://doi.org/10.1016/j.automatica.2020.109052

[19] Mohseni, N., and Bernstein, D. S., "Recursive Least Squares with Variable-Rate Forgetting Based on the F-Test," *2022 American Control Conference (ACC)*, IEEE, New York, 2022, pp. 3937–3942. https://doi.org/10.23919/ACC53348.2022.9867849

[20] McKeon, J. J., "F Approximations to the Distribution of Hotelling's T_0^2," *Biometrika*, Vol. 61, No. 2, 1974, pp. 381–383. https://doi.org/10.1093/biomet/61.2.381